ChemComm

ROYAL SOCIETY OF CHEMISTRY

COMMUNICATION

View Article Online
View Journal

Check for updates

Cite this: DOI: 10.1039/d1cc01650d

Received 27th March 2021,
Accepted 14th May 2021

DOI: 10.1039/d1cc01650d

rsc.li/chemcomm

Creating porosity in a trianglimine macrocycle by heterochiral pairing†

Donglin He, Rob Clowes, Marc A. Little, * Ming Liu * and Andrew I. Cooper *

Macrocycles are usually non-porous or barely porous in the solid-state because of their small intrinsic cavity sizes and tendency to close-pack. Here, we use a heterochiral pairing strategy to introduce porosity in a trianglimine macrocycle, by co-crystallising two macrocycles with opposing chiralities. The stable racemic trianglimine crystal contains an interconnected pore network that has a Brunauer–Emmett–Teller (BET) surface area of 355 $m^2 g^{-1}$.

Porous materials are widely useful in applications such as gas storage, molecular separations, and sensing of gases or vapours.[1–4] Synthetic control over pore structure and topology has been achieved for extended framework materials such as zeolites,[5] metal–organic frameworks (MOFs)[6] and covalent organic frameworks (COFs).[7] There is also a growing interest in porous molecular solids; one such example is porous organic cages (POCs),[8–10] where solid state function can be intrinsic to the molecular building units. Porous molecular crystals have some potential advantages compared with their extended framework cousins, such as their improved processibility.[11,12] In general, however, it is also more challenging to design structure and hence function for porous molecular solids because their crystal packing is often dictated by the sum of a variety of relatively weak and often non-directional intermolecular forces.

Macrocycles, whose solution-phase host–guest chemistry has been studied extensively,[13] have been explored recently for a range of molecular separations using the macrocycles in the solid, crystalline state. For example, Janiak and co-workers reported a trianglamine macrocycle crystal with 1-D channels that absorbed ethanol.[14] We reported a trianglimine macrocycle crystal that can separate ethyl acetate from its azeotropic mixture with ethanol.[15] Eddaoudi and co-workers reported a triangleamine-based supramolecular organic framework that showed permanent porosity and high affinity for CO_2.[16] We also reported formally non-porous pillar[*n*]arenes that selectively adsorbed styrene from ethylbenzene[17] and *para*-xylene from its structural isomers.[18] However, a challenge to the practical use of macrocycles as adsorbents for separations is their limited adsorption capacities and (often) slow adsorption kinetics. One strategy to solve these kinetic and capacity problems is to increase the porosity in the molecular system. For example, 3-D POCs, with larger cavities can exhibit Brunauer–Emmett–Teller surface areas (SA_{BET}) as high as 3758 $m^2 g^{-1}$.[19,20] It is more challenging to introduce significant porosity into macrocycles. This is because macrocycles have lower dimensional intrinsic porosity; they are also prone to close packing, minimizing any void space in the solid state.[21,22] Hence, unlike POCs with 3-D intrinsic connected pores in the solid state, macrocycle solids rarely have interconnected pore networks that facilitate the rapid diffusion of guest molecules. To date, examples of macrocycles that have been reported with a specific surface area higher than 100 $m^2 g^{-1}$ are still rare.[18,23] There is also potential benefit in accessing porous macrocycle crystals with porosity levels that are high enough to permit good diffusion kinetics while retaining the small and size/shape-specific cavity of the macrocycle.

One approach to create porosity in macrocycle structures is to introduce ''extrinsic'' pores that connect to the small intrinsic macrocycle pores.[24] Modular co-crystallization strategies have proven to be effective here.[22] For example, the modular assembly of POCs of opposing chiralities has made it possible to control the size and shape of pores in POC crystals.[25,26] The same approach also allowed 'gating POCs' to be combined with a second POC to exclude a competitive guest and to achieve high guest selectivity.[27] However, to our knowledge, this method has not been applied to control the solid state porosity of intrinsically porous molecules, other than POCs.

Isotrianglimine [3+3] macrocycles, formed by reacting isophthalaldehyde with aliphatic diamines, were first reported by Gawronski and co-workers in 2000.[28] Subsequently, a series of

Materials Innovation Factory and Chemistry Department, University of Liverpool, Liverpool, L7 3NY, UK. E-mail: aicooper@liverpool.ac.uk

† Electronic supplementary information (ESI) available. CCDC 2073632–2073637. For ESI and crystallographic data in CIF or other electronic format see DOI: 10.1039/d1cc01650d

Open Access Article. Published on 21 May 2021. Downloaded on 6/2/2021 3:40:50 PM. This article is licensed under a Creative Commons Attribution-NonCommercial 3.0 Unported Licence.

Open Access Article. Published on 21 May 2021. Downloaded on 6/2/2021 3:40:50 PM.
This article is licensed under a Creative Commons Attribution-NonCommercial 3.0 Unported Licence.

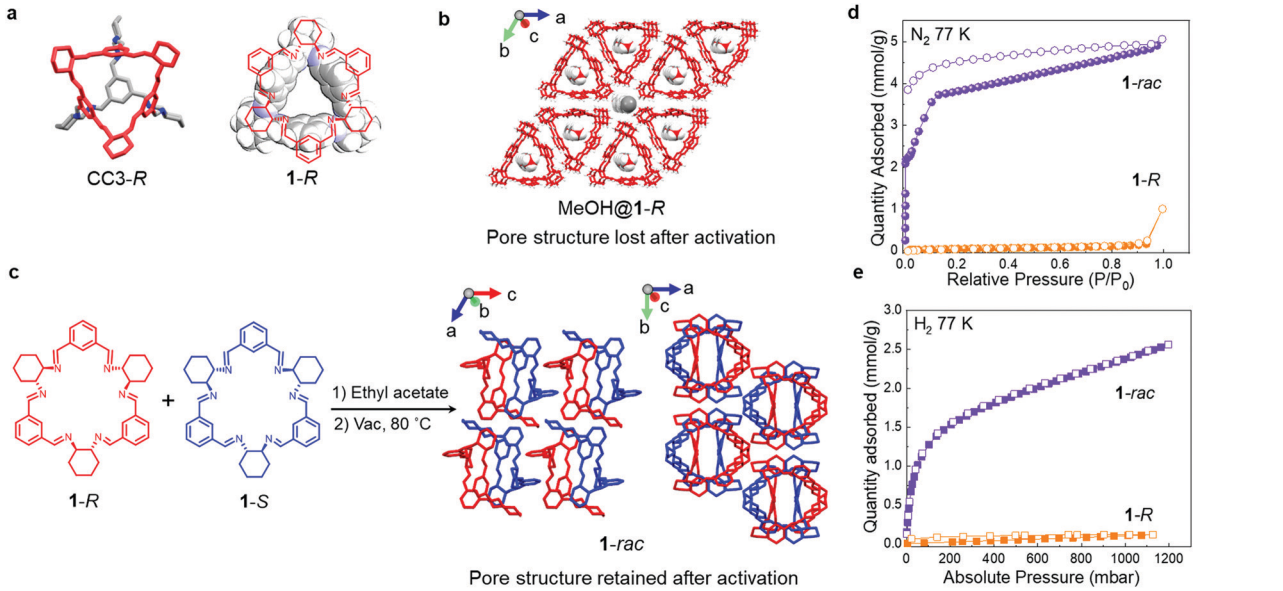

Fig. 1 (a) Single crystal structures of the chiral POC, **CC3**-*R*, which contains a structural fragment equivalent to **1**-*R* (left), and **1**-*R* (red) displayed in space filling mode (right). (b) Crystal packing in MeOH@**1**-*R*, MeOH guest displayed in space filling mode. (c) Single crystal structure of **1**-*rac*. **1**-*R* (red) and **1**-*S* (blue); H atoms are omitted for clarity. (d) N_2 and (e) H_2 sorption isotherms at 77 K for activated **1**-*R* (orange) and **1**-*rac* (purple). Solid symbols: adsorption; hollow symbols: desorption.

chiral isotrianglimines were developed, formed by the condensation of *trans*-1,2-cyclohexanediamine with substituted isophthalaldehydes were reported,[29,30] including **1**-*R* (Fig. 1a) that is synthesised by reacting *trans*-1,2-cyclohexanediamine with isophthalaldehyde. The structure of **1**-*R* is reminiscent of the window motif in the chiral POC **CC3**-*R* (Fig. 1a), which we showed to direct the crystal packing of POCs by generating energetically favourable heterochiral window-to-window packing motifs in racemic crystals.[26]

Here, we obtained solvated single crystals of **1**-*R* from methanol (MeOH@**1**-*R*, Fig. 1b) that revealed the **1**-*R* molecules were stacked in an eclipsed fashion along the crystallographic *c*-axis. This motif gave rise to pillars of **1**-*R* that contained MeOH in their intrinsic cavities. In this structure, the neighbouring **1**-*R* pillars are linked by intermolecular hydrogen bonding interaction *via* the methanol solvent molecules. It was therefore unsurprising that the packing of **1**-*R* changed when the MeOH molecules were removed from the MeOH@**1**-*R* crystals (Fig. S7, ESI†) to afford a polycrystalline **1**-*R* sample that was confirmed to be non-porous to both N_2 and H_2 (Fig. 1d and e).

Solvated racemic co-crystals of **1** (EA@**1**-*rac*) were obtained by recrystallising an equimolar ratio of **1**-*R* and **1**-*S* from ethyl acetate (EA, Fig. 1c). These crystals were found to remain suitable for single crystal analysis after activation under a dynamic vacuum at 80 °C. In the activated structure, **1**-*rac*, the racemic window-to-window packing between macrocycles is stabilised by π–π stacking and C–H···π interactions, and this was retained after removing the EA solvent (Fig. 1c and Fig. S8, S12, ESI†). The assembly of neighbouring **1**-*rac* heterochiral pairings along the *c*-axis generates interconnected pores in the crystal structure that occupy 11.6% of the unit cell, as calculated using Platon with a probe radii of 1.2 Å (Fig. 1c), with the largest free sphere (D_f) of 2.31 Å calculated by Zeo++.[31] It should be noted that the **1**-*R* structure crystallised from EA was also barely porous to N_2 and H_2 after activation (Fig. S7, S17a and b, ESI†), highlighting the importance of the racemic pairing motif for generating porosity in **1**-*rac*.

To evaluate the gas sorption properties of **1**-*R* and **1**-*rac*, we used the probe gases, N_2, H_2, and CO_2. The N_2 isotherms (Fig. 1d) show that **1**-*rac* is porous to N_2, with an apparent SA_{BET} of 355 $m^2\ g^{-1}$, and that it undergoes low-pressure adsorption step at 0.66 mbar. By contrast, **1**-*R* is essentially non-porous to N_2 and has a much lower apparent SA_{BET} of 4 $m^2\ g^{-1}$.[32] **1**-*rac* also has a much higher H_2 uptake at 1 bar and 77 K (2.56 mmol g^{-1} for **1**-*rac vs.* 0.12 mmol g^{-1} for **1**-*R*) with no hysteresis found for either sample (Fig. 1e). The gas sorption isotherms confirm that we successfully created porosity in macrocycle **1** by using the heterochiral pairing strategy to stabilise a porous crystal packing.

For materials containing very small or disconnected pores, which N_2 molecules cannot access at cryogenic temperatures, CO_2 isotherms are often used to probe porosity.[33] For **1**-*R*, the rapid onset of CO_2 adsorption isotherm at very low pressure at 195 K indicates the presence of ultra-fine pores that cannot be accessed by N_2 molecules at 77 K (Fig. S17a, ESI†).[34] CO_2 uptake for **1**-*rac* shows a typical type-I isotherm with no hysteresis loop at 195 K; at 1 bar, **1**-*rac* absorbed significantly more CO_2 than **1**-*R* (3.80 mmol *vs.* 2.17 mmol) (Fig. 2a). This result is consistent with the N_2 isotherms and confirms that substantial additional porosity has been created in **1**-*rac*. The high pressure CO_2 adsorption isotherm of **1**-*rac* at 273 K shows two successive 'plateaus' (Fig. 2b), which corresponds to CO_2 accessing the different pores in the flexible **1**-*rac* structure as it expands, and

 This journal is © The Royal Society of Chemistry 2021

Open Access Article. Published on 21 May 2021. Downloaded on 6/2/2021 3:40:50 PM.
This article is licensed under a Creative Commons Attribution-NonCommercial 3.0 Unported Licence.

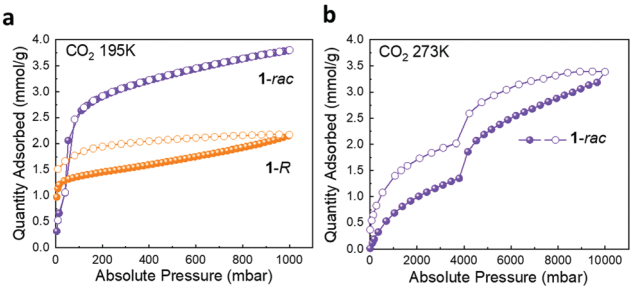

Fig. 2 CO_2 isotherms of **1**-*rac* (violet) and **1**-*R* (orange): (a) CO_2 isotherms at 195 K form 0–1 bar. (b) CO_2 isotherms at 273 K from 0 to 10 bar. Adsorption isotherms as closed symbols; desorption isotherms as open symbols.

similar behaviour has been observed in other porous solids.[35] At 273 K, 283 K, and 298 K, **1**-*R* adsorbs more CO_2 than **1**-*rac* in the low relative pressure range (0–1 bar). To understand this initially counterintuitive phenomenon, the isosteric heats of adsorption (Q_{st}) were calculated from the CO_2 isotherms (273–298 K, 0–1 bar) for **1**-*rac* and **1**-*R*. As shown in Fig. S17d (ESI†), the calculated isosteric heats of adsorption (Q_{st}) for **1**-*R* and **1**-*rac* were less than 30 kJ mol^{-1}, excluding chemisorption by either adsorbent.[36] The Q_{st} for CO_2 on **1**-*R* remained constant over a larger adsorbate loading range (0–1 mmol g^{-1}) indicating an energetically homogeneous surface.[37] **1**-*rac* had a linear decrease in Q_{st} with CO_2 loading over the range of 0–0.5 mmol g^{-1}, indicating that **1**-*rac* is more energetically heterogeneous for the adsorption of CO_2.[37] The higher CO_2 uptake of **1**-*R* at lower pressures can be attributed to ultra-fine pores in **1**-*R* that can adsorb CO_2 as a monolayer. By contrast, the larger interconnected pores of **1**-*rac* lead to the multilayer adsorption of CO_2 but with lower uptakes at lower pressures.

The separation of xylene isomers is challenging because they have similar molecular structures and physical properties. Recently, molecular materials such as cucurbit[7]uril[38] and the polymorphic azobenzene cage[39] have been studied as adsorbents for the separation of xylene isomers. The largest included sphere along the free sphere path (D_{if}) calculated by Zeo++[31,40] in activated **1**-*rac* is 4.26 Å, which is close to the molecular size of *para*-xylene (*p*X) (4.2 × 6.8 Å) (Table S1, ESI†). This close size match suggested that **1**-*rac* might be a good host for *p*X over its structural isomer, *meta*-xylene (*m*X, Table S1, ESI†). We initially crystallised **1**-*R* and **1**-*S* from *p*X and found the resulting inclusion complex, 1*p*X@**1**-*rac* (Fig. 3a). The crystal structure of 1*p*X@**1**-*rac* revealed that one *p*X molecule crystallised in the centre of the cavity created between **1**-*R* and **1**-*S* molecules packed in a window-to-window arrangement. A second *p*X molecule in the structure was located in an extrinsic void created between four **1** molecules. Compared with the guest-free structure of **1**-*rac*, the inclusion of *p*X does not significantly change the packing of **1** (Fig. 3a), as confirmed by the crystal packing overlay shown in Fig. 3b. However, **1**-*rac* does expand by around 8% to accommodate 1 mol mol^{-1} of *p*X in its structure. By contrast, the inclusion complex, 3*m*X@2(**1**-*rac*), has a different packing mode compared to activated **1**-*rac* (Fig. S9a, S14, and S16, ESI†). These results suggest that a

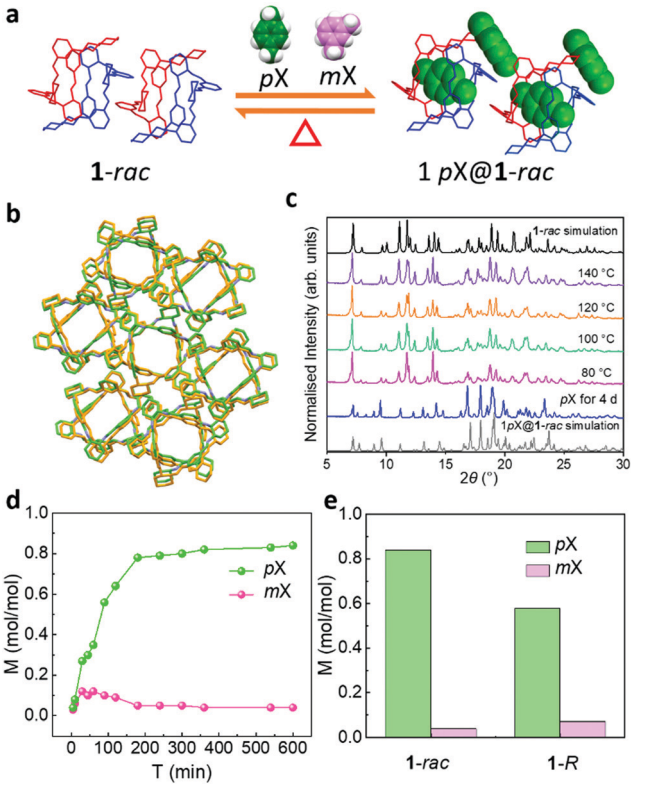

Fig. 3 (a) Reversible capture of *p*X from 1 : 1 *p*X–*m*X vapour mixture illustrated by single-crystal structures for **1**-*rac* (left) and **1***p*X@**1**-*rac* (right). **1**-*R* and **1**-*S* are coloured red and blue, respectively; H atoms are omitted for clarity. (b) Crystal packing overlay for **1***p*X@**1**-*rac* (green) and activated **1**-*rac* (yellow). (c) PXRD patterns of **1**-*rac* after being exposed to *p*X vapour and then dried under vacuum at elevated temperatures. (d) Time-dependent **1**-*rac* solid–vapour sorption plot for *p*X and *m*X equimolar vapour mixture. (e) The capacity of **1**-*R* and **1**-*rac*, determined using a 1 : 1 *p*X–*m*X vapour mixture.

racemic mixture of **1** can form inclusion complexes with both *p*X and *m*X isomers, but that the crystal packing in guest-free **1**-*rac* is more closely matched for *p*X inclusion. When we activated 1*p*X@**1**-*rac* and 3*m*X@2(**1**-*rac*) they transformed into the **1**-*rac* structure at 80 °C and 140 °C, respectively (Fig. 3c and Fig. S9a, ESI†), indicating that **1**-*rac* is the energetically favourable phase. However, the lower activation temperature for 1*p*X@**1**-*rac* indicates that *p*X desorbs more easily from 1*p*X@**1**-*rac* (Fig. S6, ESI†), which is likely due to the more interconnected 1-D porosity in 1*p*X@**1**-*rac* (Fig. 3b) and the narrower dimensions of *p*X.

To determine if **1**-*rac* could separate *p*X from *m*X, we performed time-dependent solid–vapour sorption experiments using the vapours generated from a physical mixture of the two xylene isomers. As shown in Fig. 3d, porous **1**-*rac* captures *p*X selectively from a 1 : 1 (vol : vol) mixture of *p*X and *m*X. The maximum uptake of *p*X with **1**-*rac* was 0.83 mol mol^{-1} after 10 h, which is close to the ideal ratio of 1 in 1*p*X@**1**-*rac*. The capacity of **1**-*rac* for *p*X in 1 : 1 *p*X–*m*X vapour mixture is about 1.5 times higher than for **1**-*R*, which we attribute to the increased porosity in **1**-*rac* (Fig. 3e). A larger difference, however, is in the adsorption kinetics. For example, a formally

Open Access Article. Published on 21 May 2021. Downloaded on 6/2/2021 3:40:50 PM.
This article is licensed under a Creative Commons Attribution-NonCommercial 3.0 Unported Licence.

non-porous pillar[6]arene macrocycle that adsorbs *p*X over *m*X with similar selectivity was found to reach saturation after 20 hours.[18] **1**-*rac* performs much better than this, reaching saturation after only 3 hours under the same conditions, with a selectivity coefficient of $K_{pX:mX}$ = 15.7.[41] The greatly improved adsorption kinetics of **1**-*rac* compared to the pillar[6]arene system is a direct result of its increased porosity, which results from the chiral pairing strategy.

In conclusion, we have introduced porosity into a trianglimine macrocycle system by using a heterochiral pairing strategy. Porosity was created by co-crystallising two macrocycles with the opposing chiralities such that they pack in a window-to-window arrangement to connect the intrinsic macrocycle voids. This generates an interconnected pore network with an apparent SA_{BET} of 355 m^2 g^{-1}. This is the highest reported surface area for the trianglimine macrocycle,[16,23] which are usually barely porous in the solid state. Because of its increased porosity, the **1**-*rac* co-crystal has greatly improved adsorption kinetics and shows the potential to separate xylene isomers, exhibiting much higher selectivity toward *p*X, by a factor of 15.7 *vs.* *m*X, outperforming related macrocyclic systems for the same separation.[18] As well as introducing porosity, the heterochiral pairing strategy could also enrich the functionality of these macrocycle systems by enabling hybrid mixing of macrocycles with different functions that would otherwise not co-crystallise, as demonstrated with POCs for quantum sieving applications.[42]

The authors acknowledge the EPSRC (EP/N004884/1) and the Leverhulme Trust *via* the Leverhulme Research Centre for Functional Materials Design for funding. D. H. thanks the Oversea Study Program of Guangzhou Elite Project provided by Guangzhou City, China for financial support.

Conflicts of interest

There are no conflicts to declare.

Notes and references

1 C. Sapsanis, H. Omran, V. Chernikova, O. Shekhah, Y. Belmabkhout, U. Buttner, M. Eddaoudi and K. N. Salama, *Sensors*, 2015, **15**, 18153–18166.
2 M. G. Rabbani and H. M. El-Kaderi, *Chem. Mater.*, 2012, **24**, 1511–1517.
3 J.-R. Li, R. J. Kuppler and H.-C. Zhou, *Chem. Soc. Rev.*, 2009, **38**, 1477–1504.
4 M. Brutschy, M. W. Schneider, M. Mastalerz and S. R. Waldvogel, *Adv. Mater.*, 2012, **24**, 6049–6052.
5 V. M. Georgieva, E. L. Bruce, M. C. Verbraeken, A. R. Scott, W. J. Casteel, S. Brandani and P. A. Wright, *J. Am. Chem. Soc.*, 2019, **141**, 12744–12759.
6 S. Ma, X.-S. Wang, D. Yuan and H.-C. Zhou, *Angew. Chem., Int. Ed.*, 2008, **47**, 4130–4133.
7 R.-Q. Wang, X.-B. Wei and Y.-Q. Feng, *Chem. – Eur. J.*, 2018, **24**, 10979–10983.
8 T. Tozawa, J. T. Jones, S. I. Swamy, S. Jiang, D. J. Adams, S. Shakespeare, R. Clowes, D. Bradshaw, T. Hasell, S. Y. Chong, C. Tang, S. Thompson, J. Parker, A. Trewin, J. Bacsa, A. M. Slawin, A. Steiner and A. I. Cooper, *Nat. Mater.*, 2009, **8**, 973–978.
9 T. Mitra, K. E. Jelfs, M. Schmidtmann, A. Ahmed, S. Y. Chong, D. J. Adams and A. I. Cooper, *Nat. Chem.*, 2013, **5**, 276–281.
10 A. G. Slater and A. I. Cooper, *Science*, 2015, **348**, aaa8075.
11 J. R. Holst, A. Trewin and A. I. Cooper, *Nat. Chem.*, 2010, **2**, 915–920.
12 A. I. Cooper, *ACS Cent. Sci.*, 2017, **3**, 544–553.
13 F. Vögtle and E. Weber, *Host Guest Complex Chemistry Macrocycles: Synthesis, Structures, Applications*, Springer Science & Business Media, 2012.
14 A. Janiak, M. Bardziński, J. Gawroński and U. Rychlewska, *Cryst. Growth Des.*, 2016, **16**, 2779–2788.
15 D. He, C. Zhao, L. Chen, M. Little, S. Chong, R. Clowes, K. McKie, M. Roper, G. Day, M. Liu and A. Cooper, *Chem. – Eur. J.*, 2021, DOI: 10.1002/chem.202101510.
16 A. Chaix, G. Mouchaham, A. Shkurenko, P. Hoang, B. Moosa, P. M. Bhatt, K. Adil, K. N. Salama, M. Eddaoudi and N. M. Khashab, *J. Am. Chem. Soc.*, 2018, **140**, 14571–14575.
17 K. Jie, M. Liu, Y. Zhou, M. A. Little, S. Bonakala, S. Y. Chong, A. Stephenson, L. Chen, F. Huang and A. I. Cooper, *J. Am. Chem. Soc.*, 2017, **139**, 2908–2911.
18 K. Jie, M. Liu, Y. Zhou, M. A. Little, A. Pulido, S. Y. Chong, A. Stephenson, A. R. Hughes, F. Sakakibara, T. Ogoshi, F. Blanc, G. M. Day, F. Huang and A. I. Cooper, *J. Am. Chem. Soc.*, 2018, **140**, 6921–6930.
19 M. Mastalerz, *Acc. Chem. Res.*, 2018, **51**, 2411–2422.
20 G. Zhang, O. Presly, F. White, I. M. Oppel and M. Mastalerz, *Angew. Chem., Int. Ed.*, 2014, **53**, 1516–1520.
21 N. B. McKeown, *J. Mater. Chem.*, 2010, **20**, 10588–10597.
22 M. A. Little and A. I. Cooper, *Adv. Funct. Mater.*, 2020, **30**, 1909842.
23 E. Sanna, E. C. Escudero-Adán, A. Bauzá, P. Ballester, A. Frontera, C. Rotger and A. Costa, *Chem. Sci.*, 2015, **6**, 5466–5472.
24 M. J. Bojdys, M. E. Briggs, J. T. A. Jones, D. J. Adams, S. Y. Chong, M. Schmidtmann and A. I. Cooper, *J. Am. Chem. Soc.*, 2011, **133**, 16566–16571.
25 J. T. A. Jones, T. Hasell, X. Wu, J. Bacsa, K. E. Jelfs, M. Schmidtmann, S. Y. Chong, D. J. Adams, A. Trewin, F. Schiffman, F. Cora, B. Slater, A. Steiner, G. M. Day and A. I. Cooper, *Nature*, 2011, **474**, 367–371.
26 T. Hasell, S. Y. Chong, K. E. Jelfs, D. J. Adams and A. I. Cooper, *J. Am. Chem. Soc.*, 2012, **134**, 588–598.
27 T. Hasell and A. I. Cooper, *Nat. Rev. Mater.*, 2016, **1**, 16053.
28 J. Gawroński, H. Kołbon, M. Kwit and A. Katrusiak, *J. Org. Chem.*, 2000, **65**, 5768–5773.
29 N. Kuhnert, G. M. Rossignolo and A. Lopez-Periago, *Org. Biomol. Chem.*, 2003, **1**, 1157–1170.
30 A. Troć, J. Gajewy, W. Danikiewicz and M. Kwit, *Chem. – Eur. J.*, 2016, **22**, 13258–13264.
31 T. F. Willems, C. H. Rycroft, M. Kazi, J. C. Meza and M. Haranczyk, *Microporous Mesoporous Mater.*, 2012, **149**, 134–141.
32 M. Thommes, K. Kaneko, A. V. Neimark, J. P. Olivier, F. Rodriguez-Reinoso, J. Rouquerol and K. S. Sing, *Pure Appl. Chem.*, 2015, **87**, 1051–1069.
33 P. I. Ravikovitch, A. Vishnyakov, R. Russo and A. V. Neimark, *Langmuir*, 2000, **16**, 2311–2320.
34 B. D. Chandler, D. T. Cramb and G. K. Shimizu, *J. Am. Chem. Soc.*, 2006, **128**, 10403–10412.
35 P. Lama and L. J. Barbour, *J. Am. Chem. Soc.*, 2018, **140**, 2145–2150.
36 K.-J. Chen, D. G. Madden, T. Pham, K. A. Forrest, A. Kumar, Q.-Y. Yang, W. Xue, B. Space, J. J. Perry Iv, J.-P. Zhang, X.-M. Chen and M. J. Zaworotko, *Angew. Chem., Int. Ed.*, 2016, **55**, 10268–10272.
37 S. Sircar and D. V. Cao, *Chem. Eng. Technol.*, 2002, **25**, 945–948.
38 G. Zhang, A.-H. Emwas, U. F. Shahul Hameed, S. T. Arold, P. Yang, A. Chen, J.-F. Xiang and N. M. Khashab, *Chem*, 2020, **6**, 1082–1096.
39 B. Moosa, L. O. Alimi, A. Shkurenko, A. Fakim, P. M. Bhatt, G. Zhang, M. Eddaoudi and N. M. Khashab, *Angew. Chem., Int. Ed.*, 2020, **59**, 21367–21371.
40 M. D. Foster, I. Rivin, M. M. J. Treacy and O. Delgado Friedrichs, *Microporous Mesoporous Mater.*, 2006, **90**, 32–38.
41 A. M. Pivovar, K. T. Holman and M. D. Ward, *Chem. Mater.*, 2001, **13**, 3018–3031.
42 M. Liu, L. Zhang, M. A. Little, V. Kapil, M. Ceriotti, S. Yang, L. Ding, D. L. Holden, R. Balderas-Xicohténcatl, D. He, R. Clowes, S. Y. Chong, G. Schütz, L. Chen, M. Hirscher and A. I. Cooper, *Science*, 2019, **366**, 613–620.